Res Chem Intermed (2015) 41:139–149
DOI 10.1007/s11164-013-1176-2

Effect of hydrogen peroxide on the structure and photocatalytic activity of titania

Hengpeng Ye · Shaoming Lu

Received: 1 March 2013 / Accepted: 23 March 2013 / Published online: 3 April 2013

Abstract Great attention has been paid to the fabrication of TiO_2 hollow microspheres (TiO_2-HMS) with enhanced photocatalytic activity due to the low density, high surface area, good surface permeability, and greater light-harvesting capacity. In this paper, TiO_2-HMS were fabricated by a simple hydrothermal route in a $Ti(SO_4)_2$–H_2O_2 mixed solution at 180 °C for 10 h. The prepared photocatalysts were characterized by X-ray diffraction, transmission electron microscopy, scanning electron microscopy, and nitrogen adsorption–desorption isotherms. The photocatalytic activity of the photocatalysts were evaluated by degradation of Brilliant Red X3B (X3B), an anionic dye, and the formation of the photo-induced hydroxyl radicals (·OH) under UV irradiation. The presence of hydrogen peroxide not only results in the formation of TiO_2-HMS but also stimulates the phase transformation of TiO_2 from anatase to rutile. The photocatalytic activity of the photocatalyst was found to first increase and then to decrease with the increase in the amount of H_2O_2. H_2O_2 can enhance the crystallization of anatase TiO_2. However, too much H_2O_2 results in the formation of the rutile phase, which has a negative role on the photocatalytic activity of TiO_2-HMS.

Keywords Titania · Hollow microspheres · Hydrogen peroxide · Phase structure · Photocatalytic degradation

H. Ye
Institute of Environment Engineering and Science, School of Chemistry and Material Science, Key Laboratory for Catalysis and Materials Science of the State Ethnic Affairs Commissions & Ministry of Education, South Central University for Nationalties, Wuhan 430074, China

S. Lu (✉)
College of Environmental Science & Engineering, South China University of Technology, Guangzhou 510006, China
e-mail: shmlu@scut.edu.cn

Introduction

A great deal of effort has been devoted in recent years to developing oxide semiconductor photocatalysts with high activities for environmental protection procedures, such as air purification, water disinfection, hazardous waste remediation, and water purification [1–4]. Among various oxide semiconductor photocatalysts, titania has been proven to be the most suitable for widespread environmental applications due to its biological and chemical inertness, strong oxidizing power, cost effectiveness, and long-term stability against photocorrosion and chemical corrosion [4–9]. However, the efficiency of TiO_2 photocatalysis still needs to be further improved from the point of view of practical use and commerce [10–14].

Yang and Zeng first reported the controlled synthesis of TiO_2 hollow microspheres (TiO_2-HMS) via hydrolysis of acidic TiF_4 solution [15]. Recently, fabrication of TiO_2-HMS has attracted special attention due to these structures' low density, high surface area, good surface permeability, and greater light-harvesting capacity [7, 11, 16]. Higher energy conversion efficiency and/or photocatalytic activity were reported when TiO_2-HMS were used as photocatalysts [17–20].

Although a sacrificial templating method, including hard [21] and soft template [22], has usually been used for the preparation of TiO_2-HMS, the removal of templates by calcination or dissolution is time-consuming. To overcome the complexity associated with the templating method, one-pot template-free methods for hollow structures have been developed based on direct solid evacuation with Ostwald ripening [23], which is based on the self-etching [7, 24, 25] or self-transformation [26] of the inner solid core mediated by a corrosive solution. One critical condition of this method is to use fluoride compounds such as TiF_4 and NH_4F which are able to create HF under hydrothermal reaction for the etching of solid cores [2, 16, 18, 27]. To tackle the problems related to fluoride compounds, Truong et al. [28] have very recently proposed a novel fluoride-free self-templated approach to construct TiO_2-HMS using $Ti(SO_4)_2$ and H_2O_2 as starting materials in the absence of any fluoride. However, the effect of H_2O_2 on the photocatalytic activity of TiO_2-HMS has not been systematically studied.

In this paper, the effect of H_2O_2 on the morphology and photocatalytic activity TiO_2 were systematically studied by photocatalytic degradation of Brilliant Red X3B (X3B), an anionic dye (Fig. 1), and the measurement of the formation of hydroxyl radicals under UV irradiation.

Experimental

Preparation

TiO_2-HMS were prepared according to the literature [28] but modified. Typically, 7.5 mmol $Ti(SO_4)_2$ were dissolved in 65 ml of water under magnetic stirring. Then, 10 ml of H_2O_2 (30 wt%) were dropwise added into the solution. The resulted dark red solution was transferred to a 100-ml Teflon-lined autoclave, which was then sealed and kept at 180 °C for 10 h. After cooling to room temperature, the white

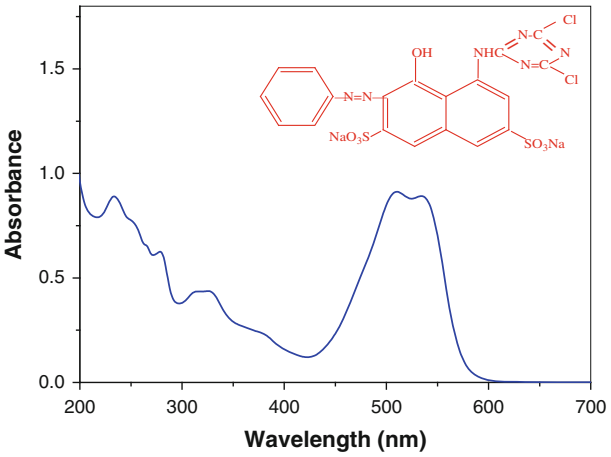

Fig. 1 Structure and electronic absorption spectrum of X3B in water

precipitate was filtrated, rinsed with distilled water, and dried in a vacuum oven at 60 °C for 8 h. For comparison, a series of TiO_2 samples were also prepared by varying the volume of H_2O_2 (from 0 to 20 ml). The prepared TiO_2 samples are labeled as Sx, where "x" represents the volume of H_2O_2 used. For examples, a TiO_2 sample prepared in the presence of 10 ml of H_2O_2 is denoted as S10, and S0 means the TiO_2 sample was fabricated in the absence of H_2O_2 (Table 1). Note that the volume of the solution in the hydrothermal reaction is kept at 75 ml for all TiO_2 samples.

Table 1 Starting materials for synthesis of the photocatalysts and the corresponding characterization results

Sample	Starting materials			Phase content[a] (%)	Crystalline size[b] (nm)	S^c_{BET} (m^2/g)
	$Ti(SO_4)_2$ (mmol)	H_2O (ml)	H_2O_2 (ml)			
S0	7.5	75	0	(AT) 100	13.8	130
S2	7.5	73	2	(AT) 100	15.1	107
S5	7.5	70	5	(AT) 84.6	(AT) 22.2	89
				(RT) 15.4	(RT) 15.7	
S10	7.5	65	10	(AT) 80.2	(AT) 36.4	54
				(RT) 19.8	(RT) 21.6	
S20	7.5	55	20	(AT) 51.6	(AT) 34.8	51
				(RT) 48.4	(RT) 15.1	

[a] AT and RT denote anatase and rutile phase, respectively

[b] Average anatase crystalline size of TiO_2 was determined by XRD using the Scherrer equation

[c] The BET surface area was determined by a multipoint BET method using the adsorption data in the P/P_0 range from 0.05 to 0.25

Characterization

The X-ray diffraction (XRD) patterns were obtained on a D8-advance X-ray diffractometer (German Bruker). The accelerated voltage and applied current were 15 kV and 20 mA, respectively. The average crystalline size of the catalyst was determined according to the Scherrer equation using full width at half maximum data after correcting for the instrumental broadening. The morphology of the TiO_2 powders was observed on a transmission electron microscope (TEM) (Tecnai G20; USA), using an acceleration voltage of 200 kV, and a field emission scanning electron microscope (SEM) (S-4800; Hitachi, Japan) with an acceleration voltage of 10 kV, respectively. Nitrogen adsorption–desorption isotherms were obtained on an ASAP 2020 (Micromeritic Instruments; USA) nitrogen adsorption apparatus. All the samples were degassed at 150 °C prior to Brunauer–Emmett–Teller (BET) measurements. The BET specific surface area (S_{BET}) was determined by a multipoint BET method using the adsorption data in the relative pressure P/P_0 range of 0.05–0.30.

Evaluation of the photocatalytic activity

The light source (375 W; Shanghai Yamin) emitted mainly at 365 nm, and was placed outside a Pyrex-glass reactor at a fixed distance (ca. 10 cm). During the photocatalytic reaction, the reactor was maintained at room temperature through a water recycle system, and was mechanically stirred at a constant rate. The concentration of TiO_2 was 1.0 g/l, and the initial concentration of X3B was 1.0×10^{-4} mol/l. Before irradiation, the suspensions were first sonicated for 5 min, and then shaken overnight in the dark. At given intervals of irradiation, small aliquots were withdrawn by a syringe, and filtered through a membrane (pore size 0.45 μm). The concentration of X3B remaining in the filtrate was then analyzed by an Agilent 8451 spectrometer at 510 nm.

The photocatalytic activity of TiO_2 was also evaluated by measurement of the formation of hydroxyl radicals in solution via a photoluminescence (PL) technique using coumarin as a probe molecule, which readily reacted with ·OH radicals to produce a highly fluorescent product, 7-hydroxycoumarin (Scheme 1) [6, 29, 30]. The suspensions of TiO_2 (1.0 g/l) containing coumarin (0.5 mmol/l) were mixed under magnetic stirring, and then shaken overnight. The following procedure is the same as that fo the degradation except that the filter was analyzed on a Hitachi F-7000 fluorescence spectrophotometer by the excitation with the wavelength of 332 nm.

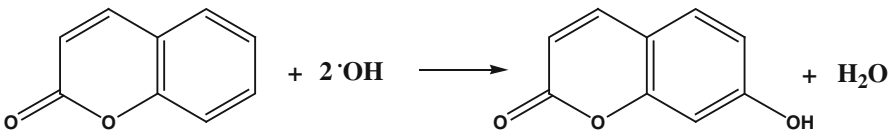

coumarin **7-hydroxycoumarin**

Scheme 1 Formation of 7-hydroxycoumarin in the reaction of coumarin with hydroxyl radicals

Results and discussion

Phase structure and morphology

Figure 2 shows the XRD patterns of the photocatalysts. A broad peak at $2\theta = 25.3°$ corresponding to the (101) plane diffraction of anatase TiO_2 was observed for all photocatalysts [29]. The peak intensity of anatase (101) diffraction increases with increasing the amount of H_2O_2 from 0 to 10 ml. According to the Scherrer equation, the crystalline sizes of anatase TiO_2 for the S0 and S10 samples are 13.8 and 36.4 nm, respectively, reflecting that the presence of H_2O_2 can enhance the crystallization of anatase TiO_2 nanocrystals. However, with further increases in the amount of H_2O_2 to 20 ml, the peak intensity of anatase (101) diffraction decreases. The crystalline size of anatase TiO_2 for S20 sample is 34.8 nm. When the amount of H_2O_2 is more than 5 ml, another peak at $2\theta = 27.4°$ corresponding to the (110) plane diffraction of rutile TiO_2 can be observed, reflecting their mixed phase [29]. The crystalline sizes of rutile TiO_2 nanocrystals were calculated to be 15.7, 21.6, and 15.1 nm for S5, S10, and S20 samples, containing 15.4, 19.8, and 48.4 % rutile phase TiO_2, respectively (Table 1). Sulfate formation of anatase TiO_2 has been reported [31], while H_2O_2 favors the formation of rutile phase TiO_2 [32]. Therefore, it is understandable that mixed phase TiO_2 was obtained in the presence of both $Ti(SO_4)_2$ and H_2O_2.

TEM (Fig. 3) was used to study the effect of H_2O_2 on the morphology of the TiO_2 sample. In the absence of H_2O_2, highly aggregated TiO_2 nanocrystals with a size of about 10–20 nm were obtained (Fig. 3a). In a small amount of H_2O_2 (2 ml), aggregated TiO_2 nanocrystals begin to form TiO_2-HMS (Fig. 3b). With the increase in the amount of H_2O_2, the formation of TiO_2-HMS can be clearly observed. Figure 3d shows the TEM image of the S10 sample. From the magnified TEM image of S10 shown in Fig. 3d, it can be seen that the TiO_2-HMS are in fact

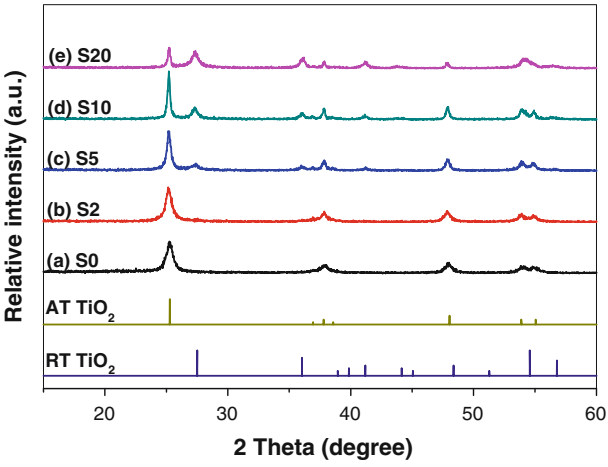

Fig. 2 XRD patterns of the photocatalysts, together with the expected diffraction peaks for anatase (*AT*) and rutile (*RT*) TiO_2, respectively

composed of nanocrystals and nanorods. Figure 4 shows the SEM image of the S10 sample. Consistent with the TEM image, the SEM image of S10 clearly shows that the TiO_2 hollow structures are aggregated nanocrystals and flower-like nanorods.

Nitrogen adsorption–desorption isotherms

The hollow structures of the synthesized TiO_2-HMS were further confirmed by nitrogen gas adsorption–desorption analysis. Figure 5 shows the effect of H_2O_2 on the adsorption–desorption isotherms and the corresponding pore size distribution curves of the photocatalysts. It can be seen from Fig. 5a that the adsorption isotherms of the photocatalyst shifted downward with an increase in the amount of H_2O_2, which infers a decrease in BET-specific surface area. By increasing the amount of H_2O_2 from 0 to 10 ml, the BET surface area of the photocatalyst steadily decreases from 130 to 54 m^2/g, which is due to the enhanced crystallization of the photocatalyst in the presence of H_2O_2 (Fig. 2). The adsorption isotherm of the S0 sample is of type IV with two capillary condensation steps, implying bimodal pore size distributions in the mesoporous and macroporous regions. According to the literature [18], a bimodal mesopore size distribution results from two different aggregates in the powders. The hysteresis loop in the lower relative pressure range ($0.4 < P/P_0 < 0.7$) is related to finer intra-aggregated pores formed between the intra-agglomerated primary particles, while the higher relative pressure range ($0.7 < P/P_0 < 1$) is associated with larger interaggregated pores produced by inter-aggregated secondary particles. This bimodal mesopore size distribution is further

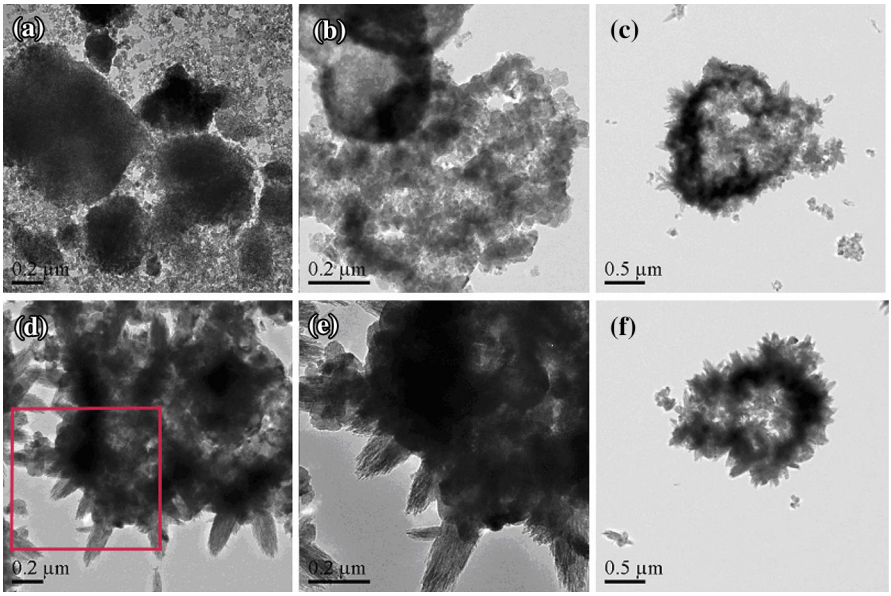

Fig. 3 TEM images of the photocatalysts: S0 (**a**), S2 (**b**), S5 (**c**), S10 (**d**), and S20 (**f**). **e** Is a magnified part of (**d**)

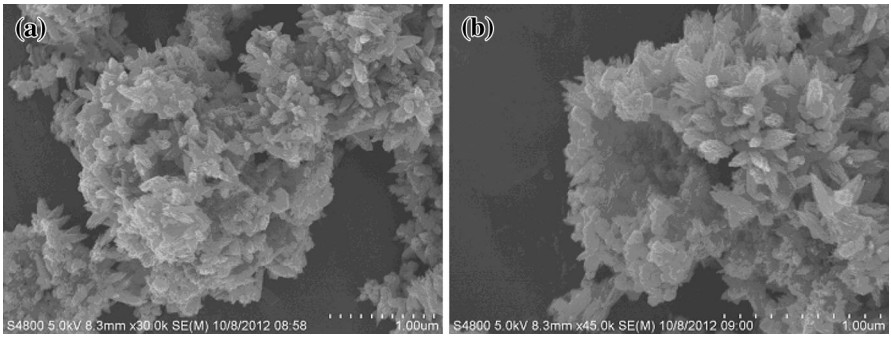

Fig. 4 SEM image of the S10 sample

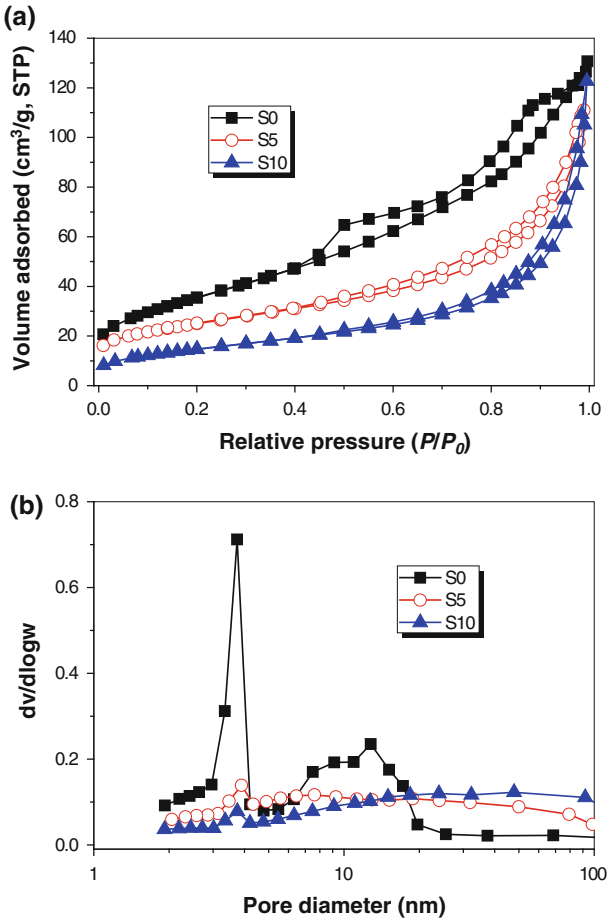

Fig. 5 Nitrogen adsorption–desorption isotherms (**a**) and the corresponding pore size distribution curves (**b**) of the photocatalysts

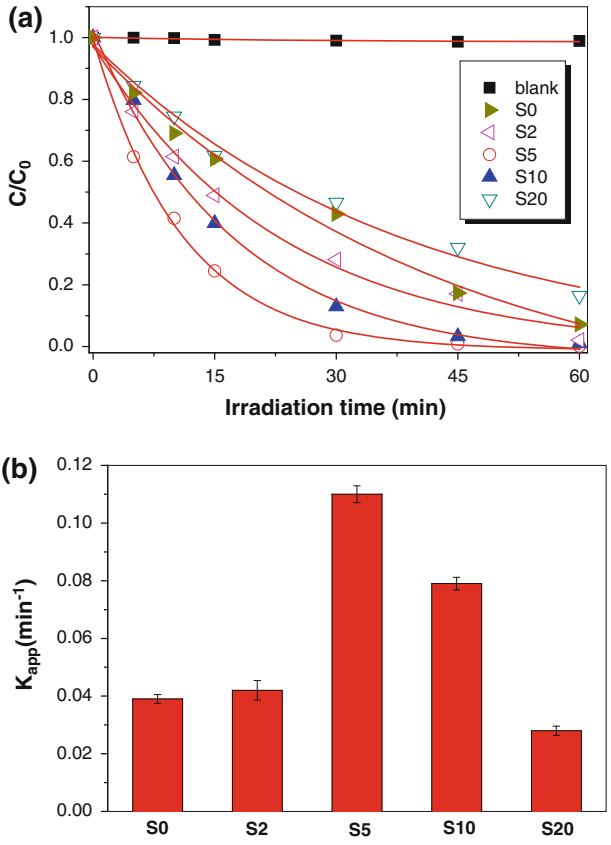

Fig. 6 Photocatalytic degradation profiles of X3B dye (**a**) and the comparison of the rate constants (**b**) in the presence of different photocatalyst

confirmed by the corresponding pore size distributions (Fig. 5b). The powder contained small mesopores (3.9 nm) and larger mesopores with a maximum pore diameter of ca. 13 nm. However, the isotherm curves of the S5 and S10 samples can be categorized as type III with only one hysteresis loop [28]. Compared with the S0 sample, the hysteresis loops of S5 and S10 shift to relatively higher pressure (0.5–1.0 P/P_0), indicating the presence of larger mesopores. This is consistent with the morphology of TiO_2-HMS (Fig. 3).

Photocatalytic activity

To study the effect of H_2O_2 on the photocatalytic activity of the photocatalyst, X3B dye was selected as an organic pollutant. Figure 6a shows the degradation profiles of X3B in the presence of different photocatalysts. It can be seen from the blank experiment that X3B is very stable, and shows little degradation under UV irradiation in the absence of TiO_2 [33, 34]. However, photocatalytic degradation of X3B becomes obvious in the presence of TiO_2. Figure 6b compares the degradation

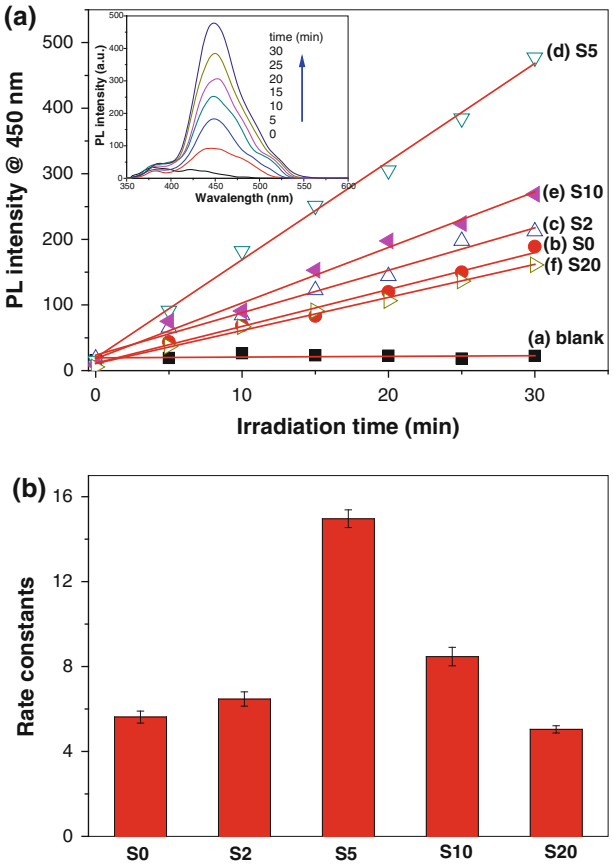

Fig. 7 Time-dependence of the induced photoluminescence intensity at 450 nm in the presence of different photocatalysts (**a**), and the comparison of the rate constants (**b**). *Inset* of (**a**) is the corresponding photoluminescence spectral changes observed during illumination of the suspensions of the S5 TiO_2 sample

rate constants. It can be seen that, with an increase in the amount of H_2O_2 from 0 to 5 ml, the degradation rate constant of X3B increases from 0.039 to 0.11 min^{-1}. The improvement of the photocatalytic activity can be ascribed to the formation of TiO_2-HMS and enhanced crystallization of anatase TiO_2 (Figs. 2, 3). There are many reports about the enhanced photocatalytic activity of TiO_2-HMS [19, 21, 24, 27, 35]. For example, the study of Truong et al. [28] showed that the hollow TiO_2 nanostructures exhibited enhanced photocatalytic activity by means of hydrogen evolution. However, the photocatalytic activity of TiO_2 was found to decrease with a further increase in the amount of H_2O_2 from 5 to 20 ml, which is probably due to the formation of rutile phase TiO_2 (Fig. 2).

Hydroxyl radicals formed in UV-illuminated TiO_2 suspensions were thought to be the main oxidative species which are responsible for the degradation of organic pollutants [29]. Here, the formation of the photo-induced hydroxyl radicals in

solution was measured by a convenient PL technique using coumarin as a probe molecule, which readily reacted with ·OH radicals to produce a highly fluorescent product, 7-hydroxycoumarin [6]. From Fig. 7, it can be seen that the slopes for the curve of PL intensity versus illumination time (rate constant), which represent the photocatalytic activity of the photocatalyst, first increase and then decrease with an increase in the amount of H_2O_2. The rate constant increases 3 times, from 5.62 for S0 to 14.96 for S5. Consistent with the degradation of X3B, the rate constant begins to decrease with further increases in the amount of H_2O_2 (decrease to 8.47 for S10 and 5.04 for S20 TiO_2 samples).

There are many factors that can affect the photocatalytic activity of TiO_2 photocatalysts, such as the crystalline phase, crystallinity, particle size, surface area, and so on [36], although the presence of H_2O_2 facilitates the production of TiO_2-HMS, which also results in the formation of rutile phase TiO_2. Compared with that of anatase TiO_2, the photocatalytic activity of the rutile phase is much lower. Therefore, it is not hard to understand the negative effects of excess H_2O_2 on the photocatalytic activity of TiO_2 samples.

Conclusions

H_2O_2 not only enhances the crystallization but also facilitate the formation of TiO_2-HMS. Small amounts of H_2O_2 play a positive role in the enhancement of the photocatalytic activity of TiO_2 due to the enhanced crystallization and the formation of TiO_2-HMS. However, excess H_2O_2 results in the production of rutile phase TiO_2, which shows poor photocatalytic activity.

Acknowledgments The authors gratefully acknowledge the financial support from National Water (Grant No. 2009ZX07423-003). Thanks are also extended to the financial support from National Natural Science Foundation of China (Project No. 41203056).

References

1. X.B. Chen, S.H. Shen, L.J. Guo, S.S. Mao, Chem. Rev. **110**, 6503 (2010)
2. K.L. Lv, B. Cheng, J.G. Yu, G. Liu, Phys. Chem. Chem. Phys. **14**, 5349 (2012)
3. J. Kim, W. Choi, H. Park, Res. Chem. Intermed. **36**, 127 (2010)
4. J.G. Yu, W.G. Wang, B. Cheng, B.B. Huang, X.Y. Zhang, Res. Chem. Intermed. **35**, 653 (2009)
5. H. Nishikiori, T. Sato, S. Kubota, N. Tanaka, Y. Shimizu, T. Fujii, Res. Chem. Intermed. **38**, 595 (2012)
6. Z.Y. Wang, K.L. Lv, G.H. Wang, K.J. Deng, D.G. Tang, Appl. Catal. B **100**, 378 (2010)
7. S.W. Liu, J.G. Yu, M. Jaroniec, J. Am. Chem. Soc. **132**, 11914 (2010)
8. K.L. Lv, Q.J. Xiang, J.G. Yu, Appl. Catal. B **104**, 275 (2011)
9. K.L. Lv, C.S. Lu, Chem. Eng. Technol. **31**, 1272 (2008)
10. Z.G. Xiong, X.S. Zhao, J. Am. Chem. Soc. **134**, 5754 (2012)
11. K.L. Lv, J.G. Yu, J.J. Fan, M. Jaroniec, CrystEngComm **14**, 7044 (2011)
12. K.L. Lv, H.S. Zuo, J. Sun, K.J. Deng, S.C. Liu, X.F. Li, D.Y. Wang, J. Hazard. Mater. **161**, 396 (2009)
13. J. Sun, X. Yan, K.L. Lv, S. Sun, K.J. Deng, D.Y. Du, J. Mol. Catal. A **367**, 31 (2013)
14. Y. Zheng, K.L. Lv, X.F. Li, K.J. Deng, J. Sun, L.Q. Chen, L.Z. Cui, D.Y. Du, Chem. Eng. Technol. **34**, 1630 (2011)
15. H.G. Yang, H.C. Zeng, J. Phys. Chem. B **108**, 3492 (2004)

16. S.W. Liu, J.G. Yu, S. Mann, Nanotechnology **20**, 325606 (2009)
17. K. Hong, K.S. Yoo, Res. Chem. Intermed. **37**, 1325 (2011)
18. J.G. Yu, S.W. Liu, H.G. Yu, J. Catal. **249**, 59 (2007)
19. X.F. Li, K.L. Lv, K.J. Deng, J.F. Tang, R. Su, J. Sun, L.Q. Chen, Mater. Sci. Eng. B **158**, 40 (2009)
20. M. Liu, K.L. Lv, G.H. Wang, Z.Y. Wang, Y.X. Zhao, Y.R. Deng, Chem. Eng. Technol. **33**, 1531 (2010)
21. X.P. Lin, D.M. Song, X.Q. Gu, Y.L. Zhao, Y.H. Qiang, Appl. Surf. Sci. **263**, 816 (2012)
22. D. Bu, H.S. Zhuang, Appl. Surf. Sci. **265**, 677 (2013)
23. X.W. Lou, L.A. Archer, Z.C. Yang, Adv. Mater. **20**, 3987 (2008)
24. X.L. Wang, H.L. He, Y. Chen, J.Q. Zhao, X.Y. Zhang, Appl. Surf. Sci. **258**, 5863 (2012)
25. L. Liu, Y.M. Cui, B. Li, X.F. Zhou, W.P. Ding, Appl. Surf. Sci. **256**, 2596 (2010)
26. C. Dwivedi, V. Dutta, Appl. Surf. Sci. **258**, 9584 (2012)
27. J.G. Yu, H.T. Guo, S. Davis, S. Mann, Adv. Funct. Mater. **16**, 2035 (2006)
28. Q.D. Truong, T.S. Lec, H.T. Hoa, CrystEngComm **14**, 4274 (2012)
29. K.L. Lv, J.G. Yu, K.J. Deng, X.H. Li, M. Li, J. Phys. Chem. Solid **71**, 519 (2010)
30. Q.J. Xiang, J.G. Yu, P.K. Wong, J. Colloid Interf., Sci. **357**, 163 (2011)
31. K.L. Lv, X.F. Li, K.J. Deng, J. Sun, X.H. Li, M. Li, Appl. Catal. B **95**, 383 (2010)
32. X.X. Li, Y.J. Xiong, Z.Q. Li, Y. Xie, Inorg. Chem. **45**, 3493 (2006)
33. Y. Zheng, K.L. Lv, Z.Y. Wang, K.J. Deng, M. Li, J. Mol. Catal. A **356**, 137 (2012)
34. K.L. Lv, J.C. Hu, X.H. Li, M. Li, J. Mol. Catal. A **356**, 78 (2012)
35. K.L. Lv, J.G. Yu, K.J. Deng, J. Sun, Y.X. Zhao, D.Y. Du, M. Li, J. Hazard. Mater. **173**, 539 (2010)
36. Y.M. Xu, K.L. Lv, Z.G. Xiong, W.H. Leng, W.P. Du, D. Liu, X.J. Xue, J. Phys. Chem. C **111**, 19024 (2007)